International Journal of Computer Information Systems and Industrial Management Applications
ISSN 2150-7988 Volume 18(4s) 2026 pp. 1098-1108
https://doi.org/10.70917/ijcisim-2026-2622
Article

Impact of Despeckling on Segmentation of Breast Ultrasonographic Images

Priyanshu Tripathi[1], Rajeshwar Dass[2], Jyotsna Sen[3]

[1]Department of Electronics and Communication Engineering (ECED), Deenbandhu Chhotu Ram University of Science and Technology (D.C.R.U.S.T.), Murthal, Haryana, India.
Email: prk.tripathi@gmail.com
[2]Department of Electronics and Communication Engineering (ECED), Deenbandhu Chhotu Ram University of Science and Technology (D.C.R.U.S.T.), Murthal, Haryana, India.
Email: rajeshwardass.ece@dcrustm.org
[3]Department of Radiology, Pt. B. D. Sharma Post Graduate Institute of Medical Sciences (PGIMS), Rohtak, Haryana, India.
Email: jyotsnasen29@gmail.com
Corresponding Author: Rajeshwar Dass,rajeshwardass.ece@dcrustm.org

Abstract: - Breast ultrasonographic imaging is a crucial imaging technique for diagnosing breast tissue abnormalities, especially in cases of dense breast tissue. However, speckle noise in breast ultrasonographic (BUS) images leads to inaccurate segmentation of anatomical structures and lesions, which further leads to inaccurate classification of breast tissue abnormalities. This study presents the impact of despeckling methods on BUS image segmentation based on image quality metric evaluation and clinical validation. In this work, first, speckle noise is reduced from BUS images of the hybrid dataset (BUSI+PGI Rohtak, HR, India), and then an efficient DL based segmentation technique is applied. The results obtained are compared with the segmentation of original images, and it is noticeable that segmentation performance in terms of mean IOU and accuracy increased from 0.904 to 0.920 and from 0.937 to 0.945, respectively, when segmentation is performed on despeckled BUS images, in spite of the original BUS images. The BUS images are carefully marked under the guidance of a Senior Professor of radiology, and the segmented BUS images are compared with the original BUS images by evaluating the overlap region in terms of mean IOU. It is observed that segmentation with despeckled images preserves diagnostic information more precisely.
Keywords: - Breast Ultrasonographic (BUS) Images, Speckle Noise, Despeckling Filters, Segmentation, Deep-Learning (DL).

1. Introduction

Ultrasonography plays a magnificent role in the diagnosis of breast tissue abnormalities, offering a non-surgical, cost-effective, and easily accessible imaging modality. However, speckle noise is a serious problem because its presence often compromises image quality and hampers accurate interpretation and further analysis [1-3].

In recent years, image segmentation algorithms have become an essential tool for delineating anatomical structures and identifying pathological regions within the breast ultrasonographic images. However, the quality of the input images has a significant impact on these segmentation algorithms. A preprocessing method called despeckling, or speckle noise reduction, has been suggested to increase image clarity and segmentation algorithm performance. Various despeckling methods, starting from mean and median filters to advanced deep learning approaches, enhanced image quality while preserving critical structural details [4-8].

This study aims to systematically investigate the effects of despeckling on the segmentation of BUS images. The findings have the potential to enhance diagnostic information and support the development of more robust computer-aided diagnosis systems in breast imaging. The findings reveal that segmentation performance is enhanced when despeckled BUS images are utilized instead of the original BUS image.

Most existing research on BUS segmentation emphasizes DL architectures but does not systematically examine the impact of despeckling on segmentation performance. The main contributions of this study are as follows:

A. This study systematically investigated the impact of speckle noise reduction on the DL-based segmentation performance of BUS images.

B. A combined dataset, that is, a benchmark dataset (BUSI) and a clinical dataset from PGI Rohtak, was used.

C. The segmentation results were also validated under the guidance of a senior radiology expert by calculating the overlap region of original image mask and corresponding despeckled image mask.

D. This study demonstrated that despeckled images retain important diagnostic information that leads to more precise lesion boundary detection.

E. A comparison between segmentation on original and despeckled BUS images is performed using mean IOU and accuracy. It highlights the effectiveness of the proposed work.

Literature Review:

A substantial amount of research has been conducted in the field of ultrasound medical imaging. Most existing studies primarily focus on objectives such as effective speckle noise suppression, preservation of edge details, and enhancement of image contrast to improve diagnostic information. The literature presented in Table 1 summarizes several significant research contributions and provides a comparative analysis of their performances.

Table 1: Summary of different studies on despeckling algorithms for ultrasonographic images.

Authors	Year	Modality Name	Despeckling algorithms	Performance evolution metrics
Ju Zhang et al. [4]	2015	BUSI	11	PSNR, SSIM & FOM
Jai Jagnath babu [5]	2016	BUSI	11	PSNR, SNR, SSIM
Kriti et al. [6]	2019	BUSI	42	IQI, Beta and SEPI
Choi et al. [7]	2020	BUSI	11	PSNR, SSIM, MSE
Gomathi et al. [8]	2022	BUSI	4	PSNR, SSIM
Ayana et al. [9]	2022	BUSI	4	PSNR, SSIM, MSE
Onur Karaoglu [10]	2022	BUSI	5	PSNR, SSIM
Yadav et al. [11]	2023	TUSI	64	IQI, Beta and SEPI
T. Ying et al. [12]	2024	BUSI	2	-
Cardona-Mesa, A.A [13]	2025	SAR Images	4	PSNR, PFOM, SSIM
Alani et al. [14]	2025	BUSI	4	PSNR, SSIM
Shuoqi Chen et al. [15]	2026	BUSI	16	PSNR, SSIM

2. Material and method

Figure 1 shows the proposed methodology and its step-by-step elaboration is as follows:

2.1. BUS Images Dataset

In this research, 752 BUS images are combined from two datasets, namely dataset A (BUSI) & dataset B (PGI Rohtak). 647 images are used from a benchmark dataset A [16]. A total of 105 images were taken from the government hospital, PGI Rohtak. These images have been collected over the years from 2021 to 2023 for an age group of 25 to 75 years. All images are also resized to 256×256 for pre-processing purposes.

2.2. Despeckling Filters

Despeckling filters are specialized image filtering methods that are used to reduce speckle noise that commonly affects medical ultrasound images. In the present study, various despeckling filters, that is, Lee, Wiener, median, bilateral, wavelet, and AD filters, were implemented, and their performance was evaluated using the structure and edge preserving index (SEPI) metric. The bilateral filter has the maximum value of the SEPI metric, as shown in Table 2 [6,15]. The structure and edge-preserving index (SEPI) is the average of IQI and β, and is given as [11]:

$$\boldsymbol{SEPI} = \frac{\boldsymbol{IQI}+\boldsymbol{\beta}}{\mathbf{2}} \qquad (1)$$

Where IQI is the image quality index, and β is a metric that measures edge preservation capabilities.

The IQI is given by [6]

$$\boldsymbol{IQI} = \frac{\boldsymbol{\sigma_{mn}}}{\boldsymbol{\rho_m \rho_n}} \cdot \frac{\mathbf{2}\bar{\boldsymbol{m}}\bar{\boldsymbol{n}}}{\bar{\boldsymbol{m}}^{\mathbf{2}}+\bar{\boldsymbol{n}}^{\mathbf{2}}} \cdot \frac{\mathbf{2}\boldsymbol{\sigma_m \rho_n}}{\overline{\boldsymbol{\sigma_m}}^{\mathbf{2}}+\overline{\boldsymbol{\rho_n}}^{\mathbf{2}}} \qquad (2)$$

where σmn is the covariance of the original & despeckled images, ρm & ρn are the standard deviations of the original and despeckled BUS images, respectively. $\bar{m}$ and $\bar{n}$ are the averages of the original and despeckled images, respectively.

The β metric is given by [17]

$$\boldsymbol{\beta} = \frac{\sum(\boldsymbol{\Delta f_m}-\overline{\boldsymbol{\Delta f_m}})(\boldsymbol{\Delta f_n}-\overline{\boldsymbol{\Delta f_n}})}{\sqrt{\sum(\boldsymbol{\Delta f_m}-\overline{\boldsymbol{\Delta f_m}})^{\mathbf{2}} \cdot \sum(\boldsymbol{\Delta f_n}-\overline{\boldsymbol{\Delta f_n}})^{\mathbf{2}}}} \qquad (3)$$

where Δf_m & Δf_n are the high-pass filtered values of the original & despeckled images, respectively

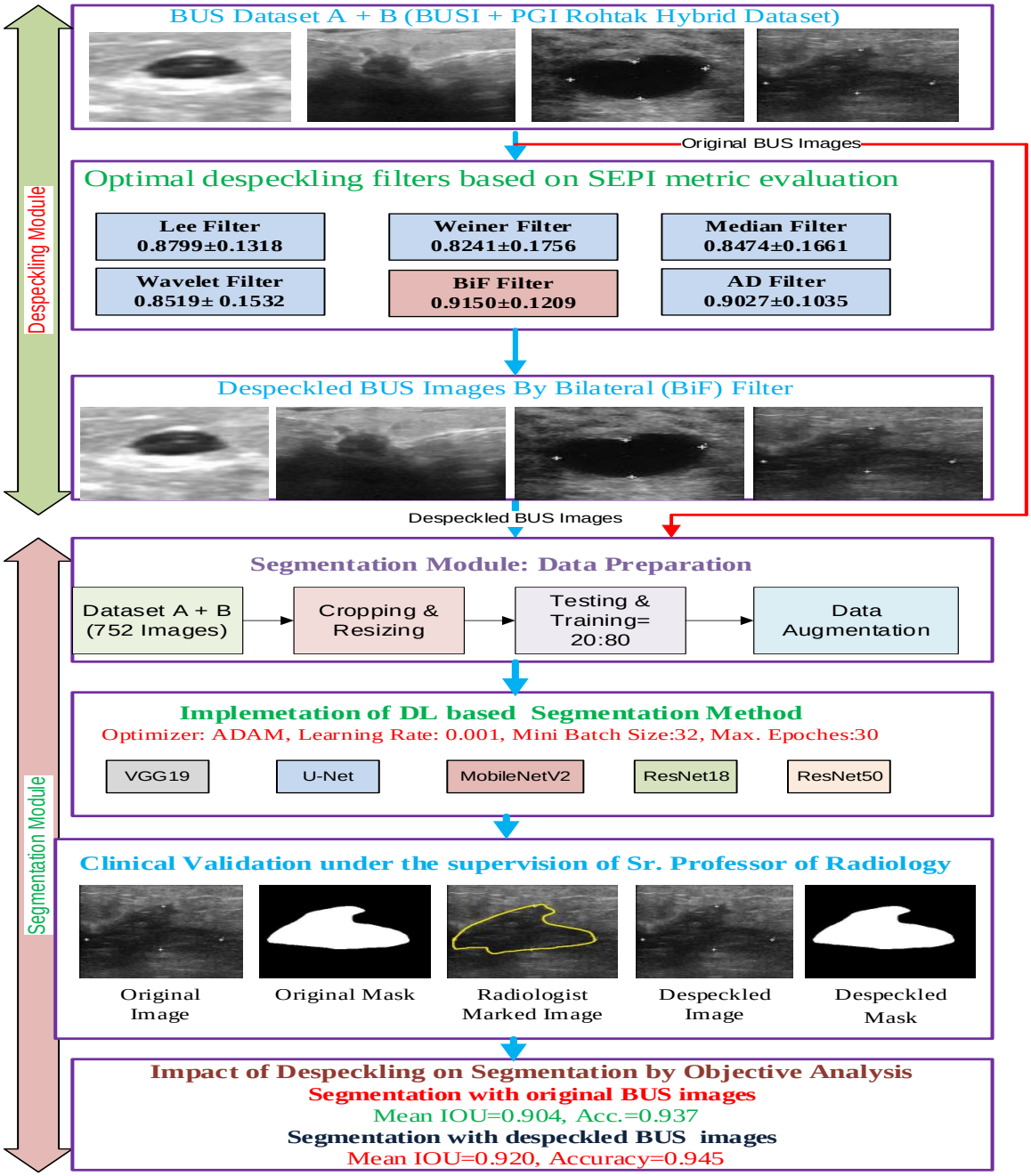

Fig.1. Methodology adopted for segmentation of BUS images

Filter Name	Parameters Used	Assessment Metrics SEPI (μ±sd)
Lee filter	Kernel size=[3x3], No. of iteration=1	0.8799±0.1318
Weiner Filter	Kernel size=[3x3], No. of iteration=1	0.8241±0.1756
Median Filter	Kernel size=[3x3], No. of iteration=1	0.8474±0.1661

Wavelet Filter	No. of iteration=1	0.8519± 0.1532
Anisotropic Diffusion (AD) Filter	No. of iteration=1, kappa=20, λ= 0.25	0.9027±0.1035
Bilateral (BiF) Filter	Degree of Smoothing=51, Spatial Sigma =2	**0.9150±0.1209**

Table 2- Specification(s) used for implementation & SEPI metric evaluation of various filters

The results of the various filters are presented in fig.2.

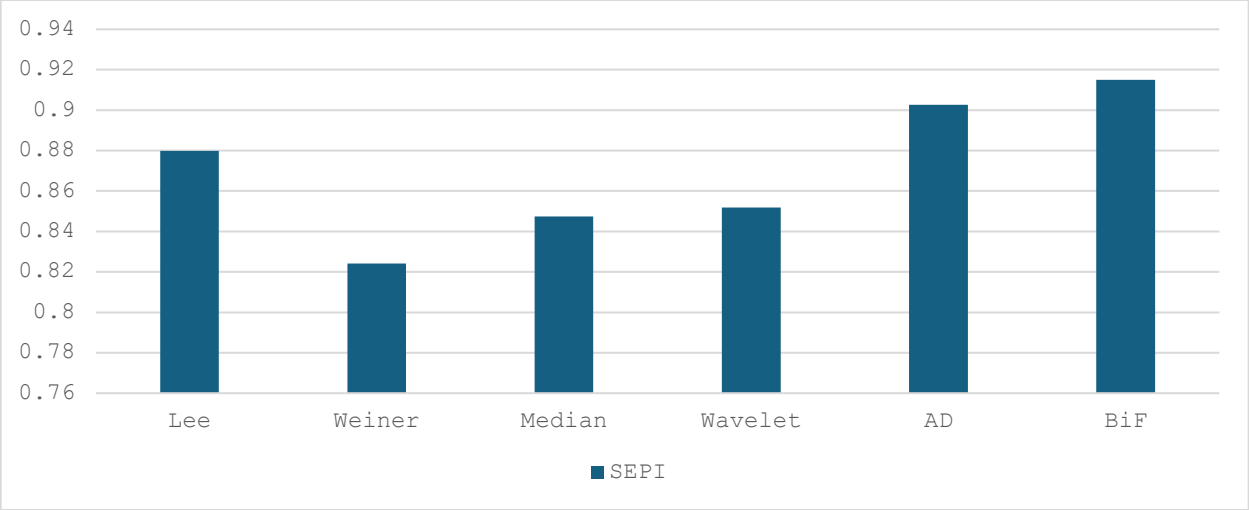

Fig. 2 - The result of different despeckling filters.

The despecked images of the various filters are depicted in fig.3.

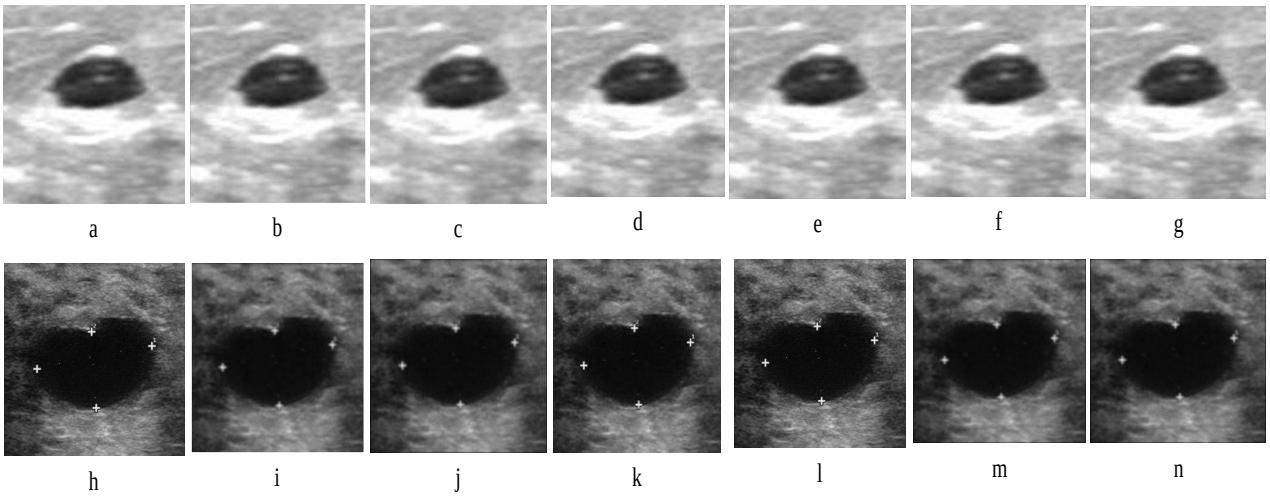

Fig.3 - (a) Original BUS Image of Dataset-A, Corresponding Despeckled Image by filters (b) Lee, (c) Weiner, (d) Median, (e) Wavelet, (f) Anisotropic Diffusion (AD), (g) Bilateral (BiF), (h) Original BUS Image of Dataset-B, Corresponding Despeckled Image by filters (i) Lee, (j) Weiner, (k) Median, (l) Wavelet, (m) Anisotropic Diffusion (AD), (n) Bilateral (BiF).

3. Segmentation Module: In this work, deep learning-based segmentation has been carried out. Many deep learning-based models are proposed by researchers, as presented in table 3 [18-26]:

Table 3: Different studies of segmentation algorithms for ultrasonographic images

S. No.	Author(s)	Year	No. of Images	Method(s)	Performance Parameter(s)
1	Samuel E. Johnny et al. [18]	2026	2500	Segment Anything Model (SAM) vision encoder	Dice = 0.887, Accuracy = 92.3%.
2	X. Xiao et al. [19]	2025	780	U-Net	Dice=0.85
3	Lal O. Boro et al. [20]	2024	-	CBAM-RIUnet	Dice=89.38% and IoU= 88.71%
5	C. Wang et al. [21]	2023	11145	ConvTrans-Net	Jaccard=85.21% Precision =85.17 Recall=89.67%
7	Kim et al. [22]	2022	1400	VGG16, ResNet34, and GoogLeNet	AUC:0.89, 0.86,0.90
8	Huang et al. [23]	2021	325+163+ 780	VGG16, ResNet101, PSPNet and Deeplab	IOU: 68.76, 75.35, 76.61, 71.58
9	Ilesanmi et al. [24]	2021	264+830	U-Net, Segnet	Dice=91.88
10	Flores et al. [25]	2020	3061	Alexnet U-Net, VGG16, VGG19, Resnet-18, Resnet-50, Mobilenet, Xception	IOU: 0.73, 0.804, 0.819, 0.826, 0.827, 0.832, 0.823, 0.821
11	Byra et al. [26]	2020	882 & 893	U-Net	Dice= 0.826 Acc=0.979

In this research, 752 images are resized to 256x256x3 for implementing VGG19, ResNet18, ResNet50, and MobileNetV2 models and then divided into testing and training datasets in the ratio of 20:80. 151 (76 benign and 75 malignant) images are utilized for testing, and the remaining 601 (421 benign & 180 malignant) images are augmented by rotation (90,180 & 270) and translation, and a total of 15626 images are prepared for training and validation. 14000 (7000 B and 7000 M) images are utilized for training, and 1626 (813 benign & 813 malignant images are utilized for validation purposes.

3.1 Implementation of DL based Segmentation Methods

In this research, different deep learning-based segmentation model implemented, viz., VGG19, ResNet18, ResNet50, MobileNetV2, and U-Net [27-36]. The ResNet50 model has the best performance among all. The basic model of ResNet50 is depicted in fig.4. ResNet50 is a widely used model for image classification and can also be implemented for image segmentation by combining either the U-Net or Deeplabv3 architecture. In this work, deeplabv3 based architecture is utilized for the implementation of ResNet50. ResNet50 is a residual-based deep learning model that uses skip connections. It utilizes four blocks, namely input, convolutional, identity, and output blocks, as depicted in fig.3(a). ResNet50 consists of two main blocks, namely the convolutional & identity blocks. The convolutional block is employed when the input & output dimensions differ from each other, providing a [1x1] convolutional layer to match the dimensions, whereas the identity block is employed when the input & output layer dimensions are already matched. In this block, input is directly added to the output. Convolutional and identity blocks are present in each stage [28]**.** The performance evaluation of segmentation methods has been carried out in terms of accuracy and mean IOU. The area of overlap region of ground truth mask and predicted mask is computed in terms of mean IOU and accuracy as given in equations 4 & 5 [36].

$$IOU = \frac{TP}{TP+FP+FN} \quad (4)$$

$$Accuracy = \frac{TP+TN}{TP+FP+TN+FN} \quad (5)$$

where TP is the true positive, TN is the true negative, FP is the false positive, and FN is the false negative.

The performance assessment of various DL-based methods is given in Table 3, and it is noticed that the ResNet50 model achieved optimal values of mean IOU & accuracy.

The Results of the different segmentation models are depicted in fig. 5.

Table 4- Performance evaluation of different segmentation methods

Model	VGG19	U-Net	MobilenetV2	ResNet18	ResNet50
Mean IOU	0. 882	0.894	0.903	0.892	**0.904**
Accuracy	0.914	0.925	0.928	0.927	**0.937**

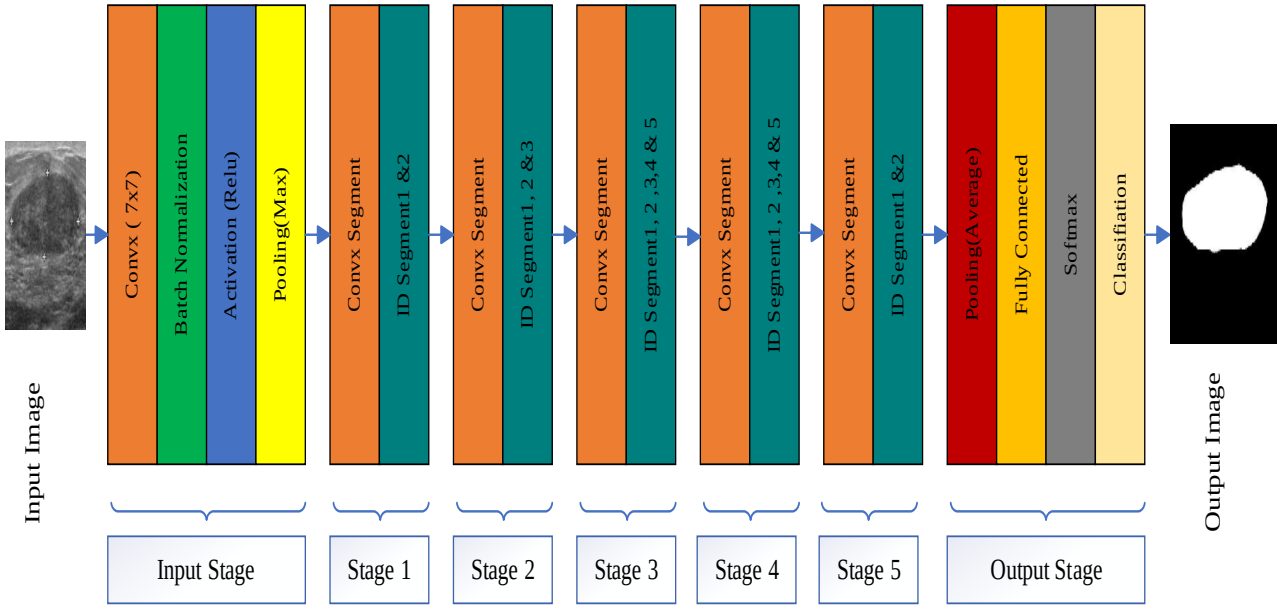

Fig. 4 – Basic ResNet50 model.

The Results of the different segmentation models are shown in Fig. 5.

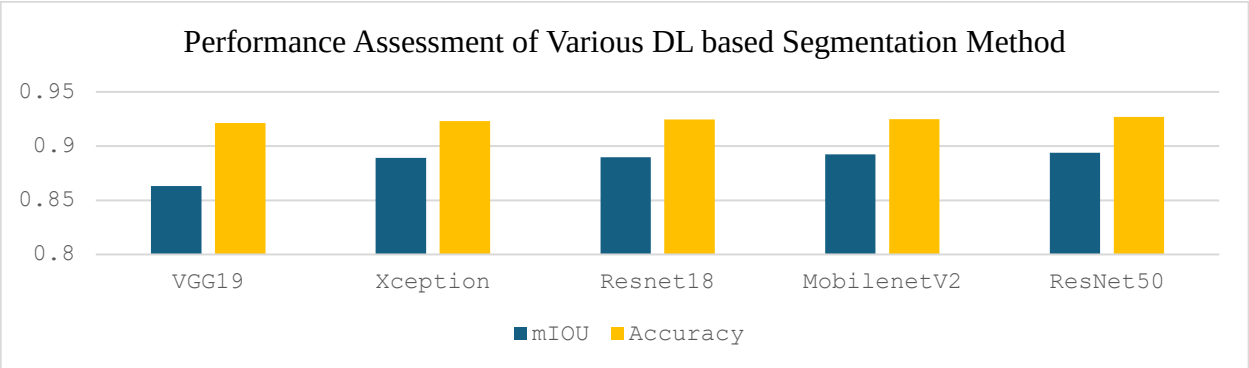

Fig. 5 - The result of different segmentation models.

3.2 Impact of despeckling on segmentation

In objective analysis, the impact of despeckling on segmentation is carried out by evaluating and comparing the mean IOU and accuracy of ResNet50 models using original & despeckled BUS images. It is observed that accuracy and mean IOU both significantly increase when segmentation is performed using despeckled BUS images rather than original BUS images, as presented in Table 5.

Table 5- Performance comparison of segmentation of original & despeckled images

Model	Mean IOU	Accuray
Original BUS Images	0.904	0.937
Despeckled BUS Images	**0.920**	**0.945**

The Result of the segmentation is presented in fig. 6.

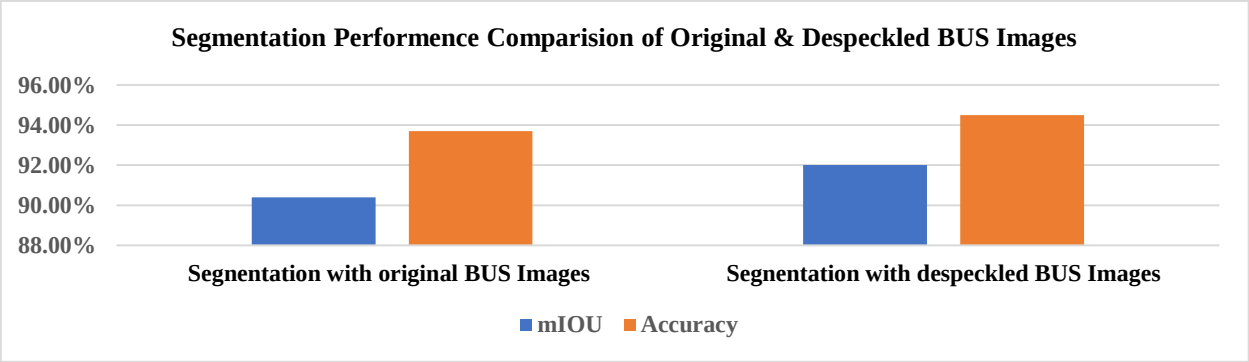

Fig. 6 - The Result of the proposed segmentation model

4. Results and Discussion:

In this research, the following experiments have performed:

A. Six different despeckling filters are applied on 752 BUS images, and their performance is computed using the SEPI metric as presented in Table 2.

B. Five DL based segmentation models are implemented using original BUS images, and their performance is evaluated using mean IOU and accuracy as shown in Table 4.

C. Optimal segmentation model, i.e., ResNet50, is also implemented using despeckled BUS images, and the results obtained are compared to the ResNet50 model using original images, as shown in Table 5.

D. The performance assessment of various DL based segmentation methods is presented in Table 3, and it is observed that ResNet50 based structure has the highest value of mean IOU, i.e., 0.904, and accuracy, i.e., 0.937.

E. To observe the impact of despeckling on segmentation, despeckled BUS images are utilized for segmentation using the ResNet50 model. The performance evaluation of segmentation of despeckled BUS images and their comparison with segmentation of original images using the ResNet50 model is listed in Table 4, and it is noticed that after despeckling, the segmentation mean IOU and accuracy increase from 0.904 to 0.920 & 0.937 to 0.945, respectively.

F. In this section, the effect of despeckling on segmentation is carried out under the guidance of a Senior Professor of the Radio-Diagnosis department. The radiologist marked the original and despeckled BUS images with their mask as depicted in fig. 7. 20 benign and 20 malignant BUS images with radiologist marking on the tumorous region were carefully reviewed by calculating the overlap region in the form of mean IOU, and it is concluded that the mask obtained from the segmentation of despeckled images preserves

diagnostic information more significantly. By comparing fig.7(h) & fig. 7 (f) and fig7(r) & fig7(o), it is observed that the mask obtained from the especkled images has sharper edges.

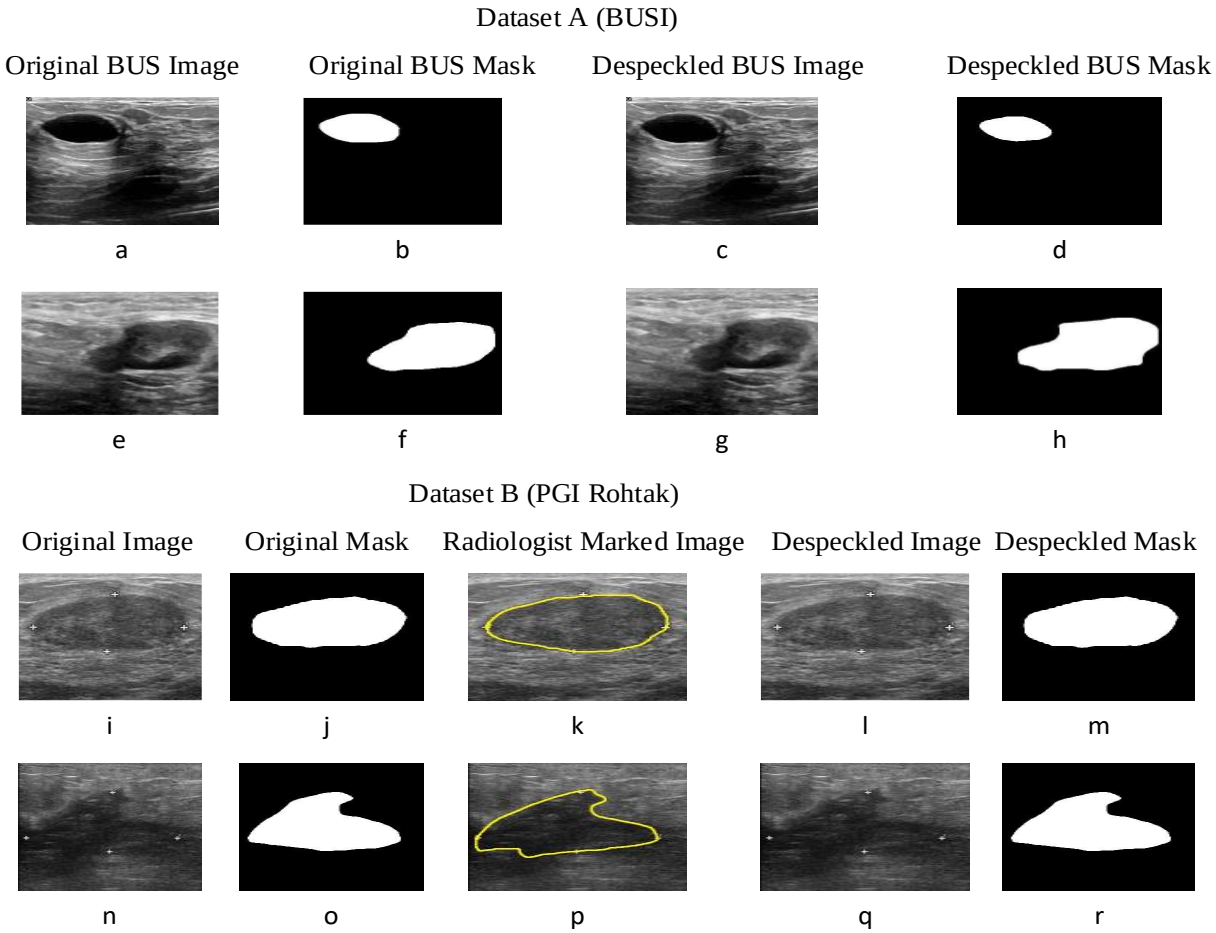

Fig.7 Breast ultrasound images with mask & corresponding segmented image with segmented mask

5. Conclusion

This work highlights the significant impact of despeckling filters on the accuracy and mean IOU of BUS image segmentation. Speckle noise, inherent in ultrasonographic imaging, often obscures critical anatomical details, impairing the performance of segmentation algorithms. By applying appropriate despeckling filters before segmentation, the image quality is significantly enhanced, leading to improved delineation of breast tissue abnormalities and lesions. This work demonstrates that despeckling not only increases contrast and reduces noise but also facilitates more accurate boundary detection and lesion localization. However, the choice of despeckling method diminishes noise with the preservation of essential image features to avoid compromising diagnostic information. Overall, effective despeckling serves as a crucial preprocessing step that significantly improves the robustness and precision of automated breast ultrasound image analysis systems, ultimately aiding in more reliable and early breast cancer detection.

In this work, different despeckling filters are implemented, and their performance is evaluated on the basis of the SEPI metric. It is concluded that the BiF filter has the highest value of SEPI metric, i.e., 0.9150. After despeckling, various DL-based segmentation models are applied on original BUS images, and the performance of these methods is evaluated using mean IOU and accuracy. It is concluded that the ReNet50 model achieved the maximum value of mean IOU, i.e., 0.904, and accuracy, i.e., 0.937. explored the effects of despeckling methods on the segmentation accuracy & mean IOU of breast ultrasonographic images. After segmentation of original BUS images, despeckled BUS images are utilized for segmentation using ResNet50, and it is concluded that effective despeckling not only

improves image quality by reducing speckle noise but also significantly enhances the performance of segmentation algorithms since mean IOU and accuracy increase from 0.904 to 0.920 & 0.937 to 0.945, respectively.

References

1. Yadav, N., Dass, R. & Virmani, J. A systematic review of machine learning based thyroid tumor characterisation using ultrasonographic images. J Ultrasound 27, 209–224 (2024).
2. Madani, M.; Behzadi, M.M.; Nabavi, S. The Role of Deep Learning in Advancing Breast Cancer Detection Using Different Imaging Modalities: A Systematic Review. Cancers 2022, 14, 5334.
3. A. Shams Rana, J. Rafique, and H. Riffat, 'Advances in Breast Ultrasound Imaging: Enhancing Diagnostic Precision and Clinical Utility', Oncology. IntechOpen, Oct. 11, 2024.
4. Zhang, J., Wang, C. & Cheng, Y. Comparison of Despeckle Filters for Breast Ultrasound Images. Circuits Syst Signal Process 34, 185–208 (2015)
5. Jai Jaganath Babu, J. Studies on Efficient Despeckling Filters for Ultrasound Thyroid Images for Improved Diagnosis. Diss. Department of Electronics and Communication Engineering, Pondicherry Engineering College, 2016..
6. Kriti, Virmani Jitendra, and Ravinder Agarwal. "Assessment of despeckle filtering algorithms for segmentation of breast tumours from ultrasound images." Biocybernetics and Biomedical Engineering 39.1 (2019): 100-121.
7. Choi, H., & Jeong, J. (2020). Despeckling algorithm for removing speckle noise from ultrasound images. Symmetry, 12(6), 938.
8. Tripathi, P., Dass, R., Sen, J. (2022). A Comparative Analysis of Different Despeckling Filters Using Breast Ultrasonographic Images. In: Marriwala, N., Tripathi, C.C., Jain, S., Mathapathi, S. (eds) Emergent Converging Technologies and Biomedical Systems . Lecture Notes in Electrical Engineering, vol 841. Springer, Singapore.
9. Ayana, G., Dese, K., Raj, H., Krishnamoorthy, J., & Kwa, T. (2022). De-speckling breast cancer ultrasound images using a rotationally invariant block matching based non-local means (RIBM-NLM) method. Diagnostics, 12(4), 862.
10. Karaoğlu, Onur, Hasan Şakir Bilge, and İhsan Uluer. "Removal of speckle noises from ultrasound images using five different deep learning networks." Engineering Science and Technology, an International Journal 29 (2022).
11. Yadav, Niranjan, Rajeshwar Dass, and Jitendra Virmani. "Despeckling filters applied to thyroid ultrasound images: a comparative analysis." Multimedia Tools and Applications 81.6 (2022): 8905-8937.
12. Ying, Tong, et al. "Breast ultrasound image despeckling using multi-filtering DFrFT and adaptive fast BM3D." Computer Methods and Programs in Biomedicine 246 (2024): 108042.
13. Cardona-Mesa, A.A.; Vásquez-Salazar, R.D.; Travieso-González, C.M.; Gómez, L. Comparative Analysis of Despeckling Filters Based on Generative Artificial Intelligence Trained with Actual Synthetic Aperture Radar Imagery. Remote Sens. 2025.
14. Alani, Omar Ayad, and Muhammad Moinuddin. "Speckle Denoising in Breast Ultrasound Images Using Multi-Filter Pseudo-Clean Targets and Deep Learning." International Journal of Advanced Computer Science & Applications 16.12 (2025).
15. Chen, Shuoqi, Yujia Wu, and Geoffrey P. Luke. "IRSDE-Despeckle: A Physics-Grounded Diffusion Model for Generalizable Ultrasound Despeckling." arXiv preprint arXiv:2602.22717 (2026).
16. https://scholar.cu.edu.eg/?q=afahmy/pages/dataset [Accessed on 20th January, 2020, 11:00 AM].
17. Rajeshwar Dass and Niranjan Yadav, "Image Quality Assessment Parameters for Despeckling Filters," ICCIDS-2019, Procedia Computer Science vol.167, Pages 2382-2392, 2020.
18. Johnny, Samuel E., et al. "Prompt-Free SAM-Based Multi-Task Framework for Breast Ultrasound Lesion Segmentation and Classification." arXiv preprint arXiv:2601.05498 (2026).
19. Xiao, X.; Zhang, J.; Shao, Y.; Liu, J.; Shi, K.; He, C.; Kong, D. Deep Learning-Based Medical Ultrasound Image and Video Segmentation Methods: Overview, Frontiers, and Challenges. Sensors 2025, 25, 2361.
20. Omega Boro L, Nandi G. CBAM-RIUnet: Breast Tumor Segmentation With Enhanced Breast Ultrasound and Test-Time Augmentation. Ultrasonic Imaging. 2024;47(1):24-36. doi:10.1177/01617346241276411.
21. C. Wang, J. Zhang and S. Liu, "Medical Ultrasound Image Segmentation With Deep Learning Models," in IEEE Access, vol. 11, pp. 10158-10168, 2023
22. Kim, J., Kim, H. J., Kim, C., Lee, J. H., Kim, K. W., Park, Y. M., Kim, H. W., Ki, S. Y., Kim, Y. M., & Kim, W. H. (2021). Weakly supervised deep learning for ultrasound diagnosis of breast cancer. Scientific Reports, 1–11.
23. Huang, K., Zhang, Y., Cheng, H. D., & Xing, P. (2021). Shape-adaptive Convolutional Operator For Breast Ultrasound Image Segmentation Utah State University , Logan , USA ; 2 Harbin Institute of Technology , Harbin , China First Affiliated Hospital of Harbin Medical University , Harbin , China. 1–6.
24. Enitan, A., Chaumrattanakul, U., &Makhanov, S. S. (2021). A method for segmentation of tumors in breast ultrasound images using the variant enhanced deep learning. Biocybernetics and Biomedical Engineering, 41(2), 802–818.
25. Gómez-flores, W., Coelho, W., & Pereira, D. A. (2020). A Comparative Study of Pre-trained Convolutional Neural Networks for Semantic Segmentation of Breast Tumors in Ultrasound, Journal P re. Computers in Biology and Medicine, 104036.
26. Byra, M., Jarosik, P., Szubert, A., Galperin, M., Ojeda-fournier, H., Olson, L., Boyle, M. O., Comstock, C., & Andre, M. (2020). Biomedical Signal Processing and Control Breast mass segmentation in ultrasound with selective kernel U-Net convolutional neural network. 61.

27. Yang, Hailong, Yinghao Liu, and Tian Xia. "Defect detection scheme of pins for aviation connectors based on image segmentation and improved RESNET-50." International Journal of Image and Graphics 24.01 (2024).
28. S. Saifullah, R. dreżewski, A. Yudhana and A. P. Suryotomo, "Automatic Brain Tumor Segmentation: Advancing U-Net with ResNet50 Encoder for Precise Medical Image Analysis," in IEEE Access, vol. 13, pp. 43473-43489, 2025
29. Uang, Q., Huang, Y., Luo, Y., Yuan, F., & Li, X. (2020). Segmentation of breast ultrasound image with semantic classification of superpixels. Medical Image Analysis, 61, 101657.
30. Yang, J., Faraji, M., & Basu, A. (2019). Robust segmentation of arterial walls in intravascular ultrasound images using Dual Path U-Net. Ultrasonics, 96(February), 24–33.
31. Karnewar, Animesh, et al. "Relu fields: The little non-linearity that could." ACM SIGGRAPH 2022 conference proceedings. 2022.
32. Yang, H., & Yang, D. (2023). CSwin-PNet : A CNN-Swin Transformer combined pyramid network for breast lesion segmentation in ultrasound images .(March), 1–7.
33. Wang R, Zhou H, Fu P, Shen H, Bai Y. A Multiscale Attentional Unet Model for Automatic Segmentation in Medical Ultrasound Images. Ultrasonic Imaging. 2023;45(4):159-174. doi:10.1177/01617346231169789.
34. Ashkani Chenarlogh V, Ghelich Oghli M, Shabanzadeh A, et al. Fast and Accurate U-Net Model for Fetal Ultrasound Image Segmentation. Ultrasonic Imaging. 2022;44(1):25-38. doi:10.1177/01617346211069882.
35. Pehrson, Lea Marie, Carsten Lauridsen, and Michael Bachmann Nielsen. "Machine learning and deep learning applied in ultrasound." Ultraschall in der Medizin-European Journal of Ultrasound 39.04 (2018): 379-381.
36. Yadav, N., Dass, R., & Virmani, J. (2023). Objective assessment of segmentation models for thyroid ultrasound images. Journal of Ultrasound, 26(3), 673-685